High-speed milling of tool steel dies for aluminium extrusion: Surface roughness, dimensional tolerance and chip removal mechanisms

High-Speed Milling of Tool Steel Dies for Aluminium Extrusion: Surface Roughness, Dimensional Tolerance and Chip Removal Mechanisms

Elena Bassoli[1], Paolo Minetola[2], and Alessandro Salmi[2]

[1]*Department of Mechanical and Civil Engineering (DiMeC), University of Modena and Reggio Emilia, Modena, Italy*
[2]*Department of Production Systems and Business Economics (DISPEA), Politecnico di Torino, Torino, Italy*

Die finishing has a fundamental importance to ensure a good quality of aluminium extruded parts and involves important economic effects due to the vastness of metalworking industry and the relatively short tool life in this field. Maximum machining efficiency is thus crucial. The research addresses optimization of finishing performances on tool steel extrusion dies. Milling tests are carried out on semimanufactured parts to ensure adherence to standard industrial technological chain, varying cutting parameters towards the field of high-speed machining (HSM). Dimensional tolerance is determined on die lands. Land surface roughness is measured through a multiscale approach and modelled as a function of cutting speed and feed. The above methodology enables a correlation between macroscopic process outcomes and chip removal mechanisms in the microscale.

Keywords AISI H13; Extrusion dies; Finishing; High-speed milling; Multiscale; Roughness; Surface quality; Tool steel.

Introduction

Tools for hot-working processes raise a great technological interest: geometry optimization, surface finish, wear reduction, and economics of machining are key issues involving important monetary effects [1–3]. The field of metalworking processes, e.g., metal die casting, hot extrusion, and hot forging, is extremely wide and involves many companies and an enormous quantity of products. Extrusion of aluminium and its alloys in complicated sections is a widespread process where the requirements in terms of products' quality and productivity are ever-increasing [1].

Surface quality of the extrudate depends on the unlubricated sliding contact between the billet's material and die lands, under high pressure and temperature. It is favored by a good surface finish of die lands and, together with dimensional tolerance, sets a limit to tool wear. Extrusion dies are made of hot work tool steels; the lands are machined to the desired finish and surface treated or covered with hard layers to reduce wear. Low die wear rates mean longer tool life, lower need for finishing operations on extruded products, fewer process stops [2]. Due to the huge amounts of extrudate and the severe working conditions on tools, technological improvements in this field are particularly incisive [2, 3], not only as to tool materials but also regarding the machining process.

A key issue towards machining optimization is to model process performances as a function of cutting parameters, so that higher cutting speed and feed can be adopted maintaining surface finish within the acceptable range [4–11]. To this aim, the field of high-speed machining (HSM) offers promising advantages that recently widened its application from aluminium alloys to tool steels [5, 6, 8, 9]. Its benefits include, besides the obvious reduction of cutting time, the chance to obtain outstanding surface quality and dimensional accuracy and to avoid further finishing operations. Several studies proved significant cost/lead time reductions by the adoption of HSM [8, 9, 12]. Nevertheless, cutting parameters maximization alone is not enough to guarantee process optimization.

Previous researches attested that significant results can be obtained adopting a multiscale approach to the study of machining operations, where traditional macroscopic indicators are merged with an investigation of micromechanisms of chip removal and tool-chip interaction. Such procedure was previously applied to several fields, where it proved to produce a better knowledge of the process and higher optimization chances [13, 14].

This research addresses the optimization of finishing performances on tool steel extrusion dies, varying cutting speed, and feed per tooth towards the field of HSM. To this aim, a set of high-speed milling tests is carried out on a hot work tool steel under dry-cutting conditions. The tests are conducted on semimanufactured parts instead of raw materials. Since the actual product is characterized by a complex 3D surface curvature, finishing operation involves variations in the uncut chip thickness and in the geometrical arrangement of tool and machined surface. Thus, tests on semimanufactured parts ensure adherence to industrial technological chain [14]. For the same reason the tool path is chosen according to industrial practice. To appraise machining quality on die lands, dimensional tolerance is determined. Moreover, surface roughness is

Address correspondence to Alessandro Salmi, Department of Production Systems and Business Economics (DISPEA), Politecnico di Torino, Corso Duca degli Abruzzi 24, Torino 10129, Italy; E-mail: alessandro.salmi@polito.il

TABLE 1.—Specifications of die material.

Classification	As supplied Hardness	After quenching Hardness	After quenching R_m [MPa]
DIN X40CrMoV5-1 (AISI H13)	220 HB	44–45 HRC	1170

measured through a multiscale approach and modelled as a function of cutting speed and feed.

EXPERIMENTAL WORK

A multihole die for aluminium extrusion is chosen as a benchmark for this study. Dies are built in hot work tool steel AISI H13, provided and machined in the annealed state whose hardness is shown in Table 1. The mechanical properties after quenching are also specified, that characterize the behavior during exercise. Dies are supplied as semimanufactured, with 0.15 mm stock on die lands.

Experiments consist of finishing operations adopting ball nose solid carbide tools shown in Fig. 1, with titanium and aluminium nitride coating. Rake and clearance angles are illustrated in Fig. 1. Milling tests are conducted on a 3-axis computer numerical control (CNC) vertical machining center (She Hong–VM 850) with maximum power of 5.5 kW. Tool path is consistent with industrial practice: Fig. 2 shows a detail of cutting geometry on the die land zone where roughness measurements are then performed. Both radial and axial cut depth are 0.15 mm. Cutting speed (v_c) and feed per tooth (f_z) adopted for finishing operation are varied through a 3^2 factorial plan in the range shown in Table 2. Starting from values typically adopted in industrial practice, both cutting speed and feed per tooth are increased through a geometric progression. The machining quality after finishing is first evaluated through dimensional and roughness measurements.

A coordinate measuring machine (CMM) is used to measure twenty uniformly distributed points on each slot. Deviation between each measurement and the nominal CAD geometry is calculated and results processed following the

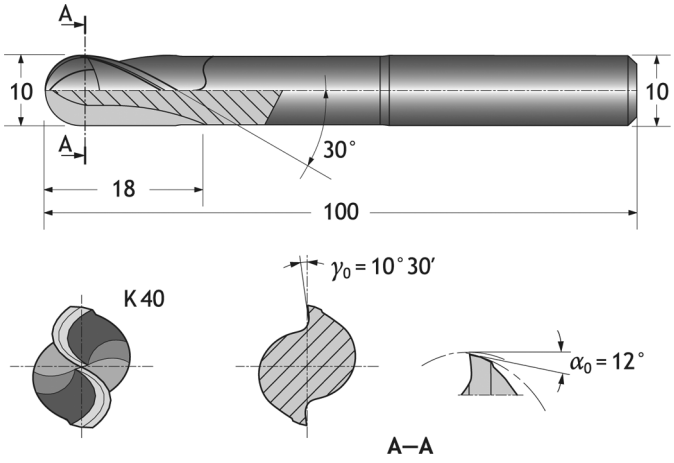

FIGURE 1.—Solid carbide end mill used for finishing operations.

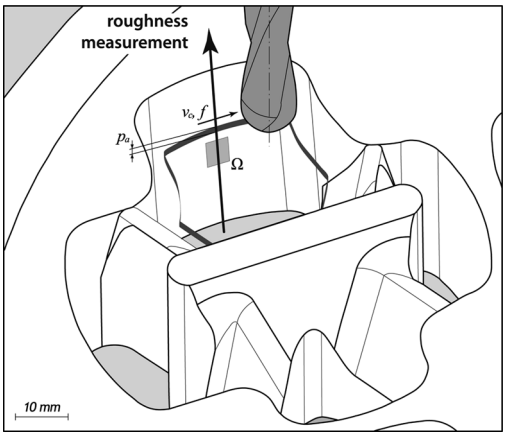

FIGURE 2.—Tool path during finishing operation and geometrical arrangement of cutting parameters and R_a measurements. Ω indicates the area of SEM and chromatic confocal microscopy (CONSCAN–CSM) observations.

tolerance unit method defined in international standards [15]. To sum up briefly, for a generic measurement D_j, known as the nominal value D_n, the number of tolerance units (n) is worked out by the dimensional deviation ($D_j - D_n$) as follows, where (i) is the standard tolerance factor:

$$n = \frac{1000 \cdot \left| D_j - D_n \right|}{i} \quad \text{with } i = 0.45\sqrt[3]{D_n} + 0.001 \cdot D_n. \tag{1}$$

Sixteen IT grades are then defined by grouping ranges of tolerance units, corresponding to as many tolerance sizes, or simply tolerances. Tolerance itself is expressed as a multiple of i. When the chi-square test proves that data distribution is non-normal, tolerance unit can be computed by 95th percentile of measurements.

Surface roughness is measured on each slot using a contact stylus profilometer (Taylor–Hobson Form Talysurf-120L). The instrument uses a Phase Grating Interferometer gauge, which ensures a nominal resolution of 12.8 nm at 10 mm range. The measurements are taken along a profile length of 4.8 mm perpendicular to the feed vector, which means parallel to the extrusion direction (Fig. 2). In particular, the following quantities are evaluated: average roughness (R_a), average maximum height of the profile (R_z), and maximum roughness depth (R_m). Average roughness values are processed by regression analysis in relation to cutting speed and feed per tooth. Several

TABLE 2.—Cutting conditions set in the 3^2 factorial plan.

		v_c [m/min]		
		130	160	200
f_z [mm/tooth · rev]	0.16	X	X	X
	0.20	X	X	X
	0.25	X	X	X

regression models are taken into account and checked using variance analysis.

On the basis of above results, the most significant experimental conditions are selected for the corresponding slots to undergo further investigations of surface roughness and morphology at a microscopic level. The following plan of experiments is adopted.

SEM Observation

The selected slots are observed through SEM using standard secondary and backscattered imaging as well as the subtraction mode of backscattered electrons (BSE). Subtraction of signals from the two detectors (A-B) allows obtaining a description of surface morphology almost independent on composition.

Surface Measurement through a High-Resolution 3D Chromatic Confocal Profilometer (CONSCAN–CSM Instruments)

The measurement is based on the optical principle of extended field stratigraphics and provides a quantitative surface characterization in the micron scale. An area of $3 \times 3\,\text{mm}^2$ is scanned acquiring 300×300 points, with a sampling rate of 300 Hz and a scan speed of 750 μm/s, using the objective active in the Z range 0–300 μm. The scan vector is parallel to the direction of macroscopic roughness profiles, that is, perpendicular to feed. Automatic filters for bad points and peaks suppression are adopted during acquisition. The resulting maps undergo the following processing protocol:

1. Form removal by subtraction of the least-squares second-order polynomial;
2. Gaussian filtering to extract waviness (cut-off length 0.8 mm);
3. Threshold filtering (bilateral symmetric) set to 0.5% removal of points, marked as unmeasured;
4. Calculation of average surface roughness S_a;
5. Five profiles' extraction perpendicular to cutting speed (length = 1.6 mm);
6. Calculation of average roughness R_a on extracted profiles.

Results and discussion

The machining quality on die lands are discussed in the following three sections, separately for dimensional tolerance and macroscale surface roughness, SEM observation, and surface measurement through a high resolution 3D chromatic confocal profilometer.

Table 3.—Results for IT grade and tolerance unit number (95th percentile).

		v_c [m/min]		
		130	160	200
f_z [mm/tooth · rev]	0.16	IT 14 ($n = 266$)	IT 15 ($n = 519$)	IT 13 ($n = 194$)
	0.20	IT 15 ($n = 469$)	IT 16 ($n = 673$)	IT 15 ($n = 501$)
	0.25	IT 13 ($n = 178$)	IT 13 ($n = 202$)	IT 14 ($n = 347$)

Dimensional Tolerance and Macroscale Surface Roughness

Table 3 shows the results of dimensional measurements processing. Results of chi-square test proved that data distribution is non-normal, so n value corresponding to 95% of observations is calculated. Tolerance unit number and IT class are shown for the nine cutting conditions. Variations of tolerance as a function of cutting speed and feed per tooth are investigated through statistical tools, proving the absence of significant correlations. Tolerance is in general quite poor for all the tests; even so, relatively low IT grades can be observed for high values of feed. This evidence suggests the intervention of excessive vibration phenomena in part of the test conditions. For this reason no further analysis is proposed as to tolerance results, whereas the study is focused on roughness and surface morphology.

Average roughness measurements from contact stylus profilometer are also examined to varying kinematic conditions, through multiple correlation analysis [16]. Two regression models are considered: complete second order polynomial and logarithmic; assuming cutting speed (v_c), feed per tooth (f_z) as independent variables. The two models can be expressed by the following equations, respectively:

$$R_a(v_c, f_z) = b_0 + b_1 v_c + b_2 v_c^2 + b_3 f_z + b_4 f_z^2 + b_5 v_c f_z \quad (2)$$

$$R_a(v_c, f_z) = \gamma v_c^{\eta} f_z^{\beta} \Rightarrow \ln R_a(v_c, f_z) = \xi + \eta \ln v_c + \beta \ln f_z \quad (3)$$

Analysis of the global correlation matrix provides negative results for the logarithmic variables, whereas p-values below the significance level ($p < 0.05$) are computed between the variables in Eq. (2). Quadratic polynomial model is thus further examined though multiple regression analysis, adopting a stepwise approach to obtain best fit of data with fewest terms. The first row in Table 4 shows the coefficients obtained with the described procedure. Four terms are computed below the level of significance: feed per tooth, square cutting speed, and feed per tooth times cutting speed; plus a constant. The model would thus include interaction between terms that are not present at the first order: this is not consistent with the principle of parsimony. Therefore, the complete model is chosen, whose coefficients are listed in the second row of Table 4. Authors are aware that cutting theory on simple geometries involves exponential equations and that a polynomial model is not representative of the process physics, but the model is only proposed as a mathematical description of the experimental figures within

Table 4.—Regression model for R_a measured by contact stylus: values of significant coefficients.

R^2_{adj}	p-level	b_0	b_1	b_2	b_3	b_4	b_5
0.97	0.00068	1.048	–	$-4.87 \cdot 10^{-5}$	–	−10.336	0.094
0.97	0.02419	−0.487	$1.13 \cdot 10^{-2}$	$-7.41 \cdot 10^{-5}$	−3.643	−10.505	0.078

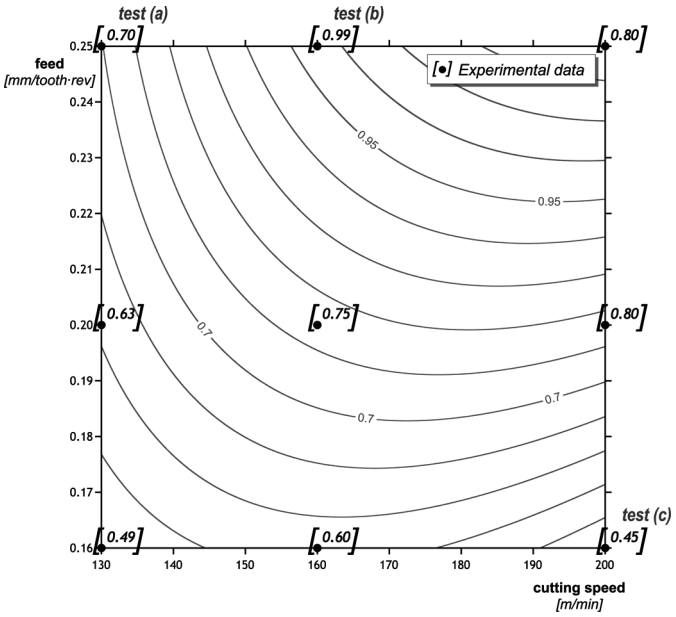

FIGURE 3.—Average roughness R_a (μm) vs. cutting speed and feed per tooth. Radial and axial depth of cut are 0.15 mm for all the tests.

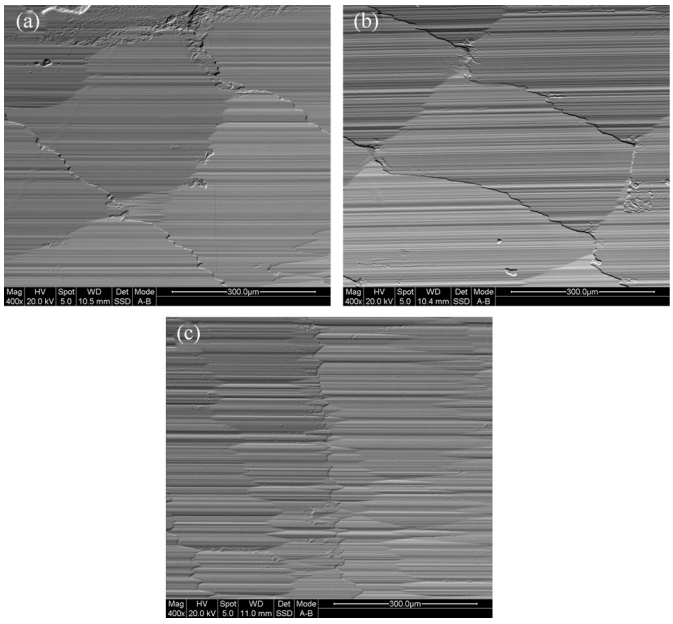

FIGURE 4.—BSE A-B image of the milled surface (refer to Ω region in Fig. 2) corresponding to: test (a) $v_c = 130$ m/min, $f_z = 0.25$ mm/tooth · rev; test (b) $v_c = 160$ m/min, $f_z = 0.25$ mm/tooth · rev; and test (c) $v_c = 200$ m/min, $f_z = 0.16$ mm/tooth · rev. Radial and axial depth of cut are 0.15 mm for all the tests.

the investigated domain of validity. Adjusted coefficient of determination (R^2_{adj}) is 0.97, proving a good fit of experimental data whose variability is explained by the regression model by 97%. The model is plotted in Fig. 3, where the experimental measurements are superimposed as black solid circles to the contour lines. The measured values show a good agreement to the model, except the boundary condition $v_c = 200$ m/min, $f_z = 0.25$ mm/tooth · rev that is excluded from further investigation, because further tests are required to understand the trend in the direction of combined high cutting speed and feed.

Commenting on roughness results, low values can be observed near the minimum feed per tooth, which matches basic cutting theory. Technical literature on HSM relates that a reduction of surface roughness can be remarked as cutting speed increases. The above behavior can be perceived in Fig. 3 in the range of low feed per tooth. Analysis of the previous results for macroscopic roughness values leads to select significant cutting conditions for a deeper investigation of the surface morphology and cutting micromechanisms. The following specimens are chosen:

1. The theoretical minimum and maximum predicted by the model that describes surface roughness as a function of the cutting parameters: test (c) [$v_c = 200$ m/min, $f_z = 0.16$ mm/tooth · rev] and test (b) [$v_c = 160$ m/min, $f_z = 0.25$ mm/ tooth · rev];
2. The lowest cutting speed and highest feed per tooth: test (a) [$v_c = 130$ m/min, $f_z = 0.25$ mm/tooth · rev]. The opposite condition coincides with the minimum theoretical roughness mentioned in the previous paragraph.

SEM Observation

The three selected surfaces are observed through SEM. Subtraction of signals from the two BSE detectors provides topography images exemplified in Fig. 4.

Commenting on the results, two distinct sources of surface unevenness can be noticed. At macroscale, the milled surfaces show memory of each tooth's action. Domains are visible whose height can be ascribed to axial depth of cut and width to feed per tooth. The described morphology is extremely clear in Figs. 4(a) and (b), where domain dimensions are identical, as can be observed in the elaboration in Fig. 5 that highlights the domain contours. This aspect is only slightly less evident in Fig. 4(c), due to the difference in local surface curvature. Surface geometry

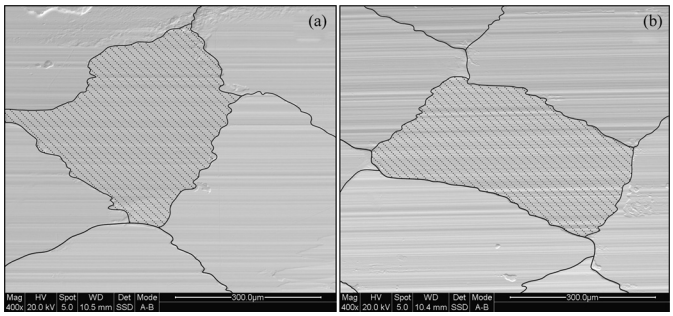

FIGURE 5.—Elaboration of the images in Fig. 4 to highlight mesh domains. Data correspond to: test (a) $v_c = 130$ m/min; $f_z = 0.25$ mm/tooth · rev and test (b) $v_c = 160$ m/min, $f_z = 0.25$ mm/tooth · rev. Radial and axial depth of cut are 0.15 mm for all the tests.

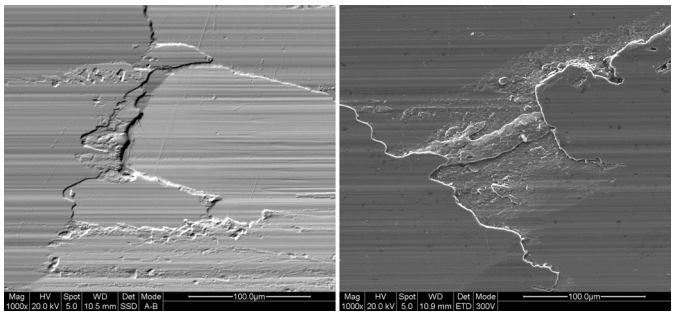

FIGURE 6.—Details of surface irregularities due to chip detach common to all cutting conditions. Radial and axial depth of cut are 0.15 mm for all the tests.

reminds of a quadrangular mesh which is finer and closer to the theoretical surface as subsequent teeth overlapping on the same area is enhanced, i.e., feed per tooth and axial cut depth decrease. Radial depth of cut would have an effect too, through the engagement angle.

Increasing the level of detail, surface morphology within each of the described domains shows edges parallel to cutting speed, depending only on the mechanisms of tool-chip interaction and chip detach. If (a) and (b) images in Fig. 4 are compared, where the first macrophenomenon leading to quadrangular domains is exactly alike, the second mechanism can be appreciated, that is, the surface morphology within each domain. A smoother surface can be noticed for $v_c = 130$ m/min than for $v_c = 160$ m/min, being $f_z = 0.25$ mm/tooth · rev, as shown in Figs. 4(a) and (b), consistent with the roughness model previously discussed. As to the cutting condition $v_c = 200$ m/min and $f_z = 0.16$ mm/tooth · rev [Fig. 4(c)], smoothness of the edges is comparable to Fig. 4(a). The lower roughness values must thus be ascribed to the smaller dimensions of the *mesh* domains related to a single tooth's action.

Figure 6 shows details of surface irregularities produced at the boundaries of tooth engagement, common to all the cutting conditions.

Surface Measurement Through a High-Resolution 3D Chromatic Confocal Profilometer (CONSCAN–CSM Instruments)

3D chromatic confocal microscope provides color maps representing surface depth on the inspected areas of the three milled surfaces, represented in Fig. 7 with the same scale. Points removed by spikes and threshold filtering, together with the undetected areas, are white in the maps. Cutting speed and feed are horizontal in the images. Surface morphology appears exactly alike the one described in the previous section. Besides, confocal profilometry measurements allow to match the previous qualitative observations with a quantitative assessment.

The overall depth range in the maps can be related to maximum roughness. The value is less than 7 μm in Fig. 7(c), whereas it increases for Fig. 7(a) and is maximum in Fig. 7(b), about twice bigger than in Fig. 7(c). The condition $v_c = 160$ m/min, $f_z = 0.25$ mm/tooth · rev provides much higher irregularities at the beginning and end of each tooth's action, where material piles up. The

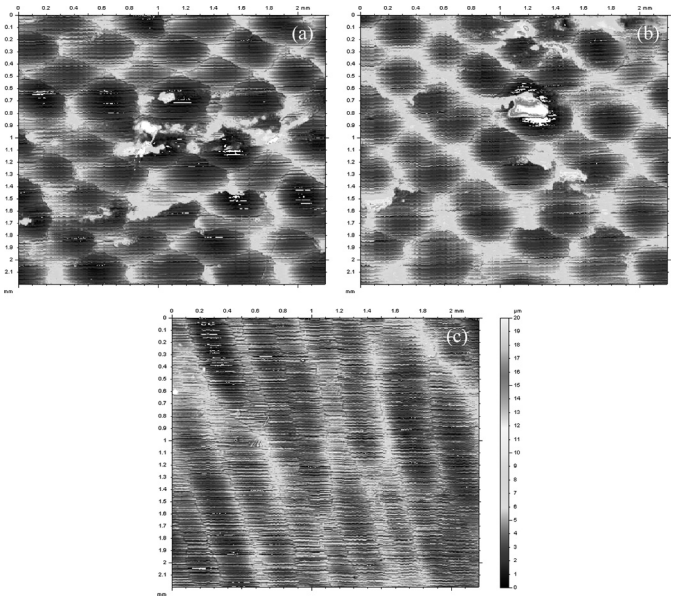

FIGURE 7.—Color maps of the surface depth measured by chromatic confocal microscopy on areas of 5×5 mm^2 (refer to Ω region in Fig. 2) corresponding to: test (a) $v_c = 130$ m/min, $f_z = 0.25$ mm/tooth · rev; test (b) $v_c = 160$ m/min, $f_z = 0.25$ mm/tooth · rev; and test (c) $v_c = 200$ m/min, $f_z = 0.16$ mm/tooth · rev. Radial and axial depth of cut are 0.15 mm for all the tests.

phenomenon is less evident if cutting speed is reduced to 130 m/min. If $v_c = 200$ m/min and $f_z = 0.16$ mm/tooth · rev, instead, a smooth surface is obtained.

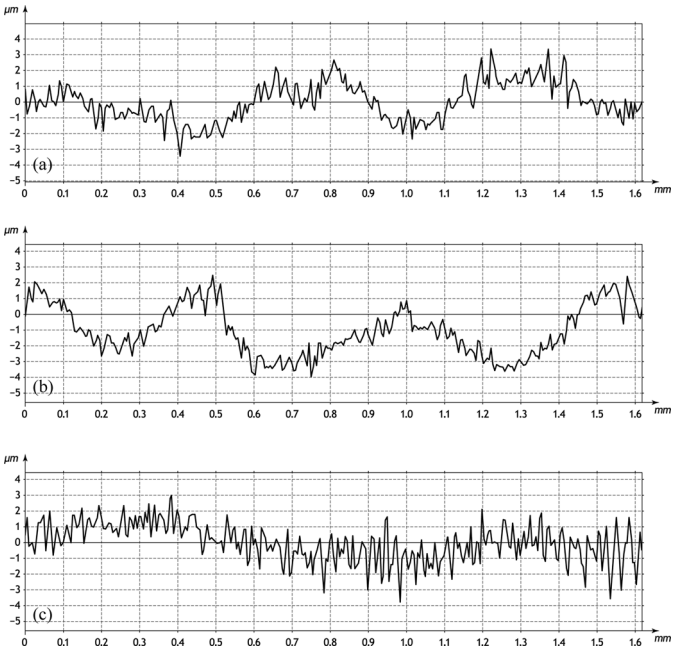

FIGURE 8.—Longitudinal profiles extracted from the maps in Fig. 7: test (a) $v_c = 130$ m/min, $f_z = 0.25$ mm/tooth · rev; test (b) $v_c = 160$ m/min, $f_z = 0.25$ mm/tooth · rev; and test (c) $v_c = 200$ m/min, $f_z = 0.16$ mm/tooth · rev. Radial and axial depth of cut are 0.15 mm for all the tests.

TABLE 5.—Surface roughness S_a and profiles roughness R_a measured by profilometry.

	$v_c = 130$ m/min $f_z = 0.25$ mm/tooth · rev	$v_c = 160$ m/min $f_z = 0.25$ mm/tooth · rev	$v_c = 200$ m/min $f_z = 0.16$ mm/tooth · rev
S_a (μm)	1.28	1.42	1.05
R_a (μm) mean (SD)	0.76 (0.11)	0.85 (0.11)	0.63 (0.07)

Profiles were extracted from the point clouds described as maps in Fig. 7, transverse with respect to cutting speed. The high level of detail offers the possibility to avoid surface defects in the generation of profiles, that is, the white areas in the maps. Figure 8 allows a comparison between three profiles of the selected specimens. The described difference in terms of surface *meshed* morphology or roughness within each edge action is clearly visible. Average surface roughness on the maps S_a and mean R_a on the extracted profiles are listed in Table 5. The values are consistent with the described mechanisms and with the macroscopic contact measurements. Cutting speed of 200 m/min and feed per tooth of 0.16 mm/tooth · rev provide minimum roughness with very narrow standard deviation.

CONCLUSIONS

The article presented an experimental investigation of finishing performances on tool steel extrusion dies using solid carbide tools and varying cutting speed and feed per tooth towards the field of high speed milling. Dimensional tolerance was determined on die lands. Land surface roughness was measured through a multiscale approach and modelled as a function of cutting speed and feed. Minimum surface roughness was around 0.5 μm, obtained for minimum feed per tooth and maximum cutting speed. The investigation with different experimental techniques proved that consistent values of macro-indicators can be obtained. Besides, the study of chip removal mechanisms in the microscale provides richer information that can be related to macroscopic process outcomes and build the basis for better optimization results.

ACKNOWLEDGMENTS

The authors would like to acknowledge the assistance of Mr. Giovanni Marchiandi and Dr. Gianluca Negro in facilitating the machining operations and measurements in this study.

REFERENCES

1. Qamar, S.Z.; Arif, A.F.M.; Sheikh, A.K. Analysis of product defects in a typical aluminum extrusion facility. Mater. Manuf. Process **2004**, *19*, 391–405.
2. Björk, T.; Westergård, R.; Hogmark, S. Wear of surface treated dies for aluminium extrusion—A case study. Wear **2001**, *249*, 316–323.
3. Navinšek, B.; Panjan, P.; Urankar, I.; Cvahte, P.; Gorenjak, F. Improvement of hot-working processes with PVD coatings and duplex treatment. Surf. Coat. Technol. **2001**, *142–144*, 1148–1154.
4. Gatto, A.; Iuliano, L.; Bassoli, E.; Violante, M.G. High speed milling of light alloys: Tool performance and chip formation analysis. 6th Biennial Conference on Engineering Systems Design and Analysis, July 8–11, 2002; Instanbul, Turkey.
5. Gatto, A.; Iuliano, L. Chip formation analysis in high speed machining of a nickel base superalloy with silicon carbide whisker-reinforced alumina. Int. J. Mach. Tool. Manu. **1994**, *34*, 1147–1161.
6. Gatto, A.; Iuliano, L.; Tagliaferri, V. High speed turning of metal matrix composites with tools of different material and geometry. Material and Design Technology **1995**, *71*, 79–85.
7. Kazban, R.V.; Mason, J.J. Fluid mechanics approach to machining at high speeds: Part I: Justification of potential flow models. Mach. Sci. Technol. **2007**, *11*, 475–489.
8. Ekinovic, S.; Dolinsek, S.; Jawahir, I.S. Some observations of the chip formation process and the white layer formation in high speed milling of hardened steel. Mach. Sci. Technol. **2004**, *8*, 327–340.
9. Toh, C.K. Surface topography analysis when high-speed rough milling hardened steel. Mater. Manuf. Process **2003**, *18*, 849–862.
10. El-Tamimi, A.M.; El-Hossainy, T.M. Investigating the machinability of AISI 420 stainless steel using factorial design. Mater. Manuf. Process **2008**, *23*, 419–426.
11. Saikumar, S.; Shunmugam, M.S. Parameter selection based on surface finish in high-speed end-milling using differential evolution. Mater. Manuf. Process **2006**, *21*, 341–347.
12. Coldwell, H.; Woods, R.; Paul, M.; Koshy, P.; Dewes, R.; Aspinwall, D. Rapid machining of hardened AISI H13 and D2 moulds, dies and press tools. J. Mater. Process. Technol. **2003**, *135*, 301–311.
13. Iuliano, L.; Violante, M.G.; Gatto, A.; Bassoli, E. Study of the EDM process effects on aluminum alloys. Int. J. Manufacturing Technology and Management, Special Issue on "Innovative approaches in Technology and Manufacturing Management" **2008**, *14*, 326–341.
14. Bassoli, E.; Iuliano, L.; Salmi, A. Deep drilling of aluminium die-cast parts: Surface roughness, dimensional tolerance and tool-chip interaction. Materials and Manufacturing Processes **2010**, *25*, 442–449.
15. UNI EN 20286-1:1995, ISO System of limits and fits. Bases of tolerances, deviations and fits.
16. Montgomery, D.C.; Ranger, G.C. *Applied Statistics and Probability for Engineers*, 2nd Ed.; Wiley: New York, 1999.